Novel method to calibrate CT scanners with a conic probe body

Tischenko O.[a], Saeednejad N. [b], Hoeschen C.[b]
[a]Medical Biokinetics and Radiation Physics, Helmholtz Zenrum Muenchen, National German Research Center for Environmental Health, Ingolstaedter Landstrasse 1, D-85764 Neuherberg, Germany
[b]Medical Systems, Otto-von-Guericke University Magdeburg, Germany

ABSTRACT

A new and simple object for calibrating tomographic scanners has been proposed. Instead of a conventional high-density ball as an object for calibration, we propose a high-density conic body. The cone is advantageous compare to the ball both because of its easy availability (uncomplicated manufacturing) and the straightforward and less error-prone analysis necessary for the identification of a space point (ball's center vs. cone apex). Applying the conic body instead of a ball as a calibration object enables to reduce calibration errors substantially. Additionally we propose an efficient way to determine the discrepancy between ideal and misaligned positions of the detector that may be crucial for the quality of the reconstruction.

Keywords: x-ray tomography, cone beam CT, calibration

1. INTRODUCTION

The quality of the reconstruction in the cone-beam tomography depends crucially on the knowledge of the scanning geometry, or in other words, on the knowledge of the spatial configuration of rays associated with the acquired data. Therefore an assessment of the geometry of a CT scanner and the calibration of its detector misalignments is a necessary task that has to be performed regularly. Different methods for estimating geometric parameters of a CT imaging system have been proposed. Many of them are based on measuring projections of a space point referred to as a calibration point [1-3]. Then the unknown geometric parameters $a_1,...,a_n$ are solutions of non-linear equations

$$f_k(a_1,...,a_n) = F_k,\ \ k = 1,...,N$$

where at the right there are the coordinates of projections of the calibration point measured in the reference system of the detector. Normally, the center of a high density ball plays the role of the space point. This affects the observations and causes errors of measurements. Since solutions of equations depend non-linearly on these errors it is important to reduce the errors of measurements as much as possible. As far as we aware, one tries to accomplish this task by means of controlling the value of a radius of the ball. The radius has to be neither too big nor too small. If it is too big the difficulty may be in the analysis of the grey value image of the ball as well as in the analysis of its shadow cast on the detector. In approaches, where one is to identify the center of mass of the ball grey value image, inhomogeneity within the ball can introduce further errors. The analysis of the ball's shadow is complicated since the shadow is an ellipse, and the center of the ball may be projected neither into the center of the ellipse nor into its focus. Therefore the radius of the ball has to be as small as possible. In this case, however, the area of the shadow becomes small such that only few pixels within the shadow can be used to identify the locus of the center of mass of the ball's image; this may cause further interpolating errors.

In order to simplify the processing task and avoid difficulties related to inhomogeneity, we propose to use instead a high density cone the apex of which can be considered as a space point. As described below, the cone does not need to have a sharp tip.

Medical Imaging 2017: Physics of Medical Imaging, edited by Thomas G. Flohr, Joseph Y. Lo, Taly Gilat Schmidt, Proc. of SPIE Vol. 10132, 101322Q · © 2017 SPIE
CCC code: 1605-7422/17/$18 · doi: 10.1117/12.2254081

2. THEORY

2.1 Identification of the projection of the apex of a conic object

As it was said in the introduction, the calibration point is the apex of the conic body. Consider the shadow cast by the cone on the detector plane. The boundary of this shadow is constituted by two straight lines which are the lines of the intersection of the detector plane and the planes that contain the focus of the x-ray source and which are tangent to the cone surface (see Fig.1).

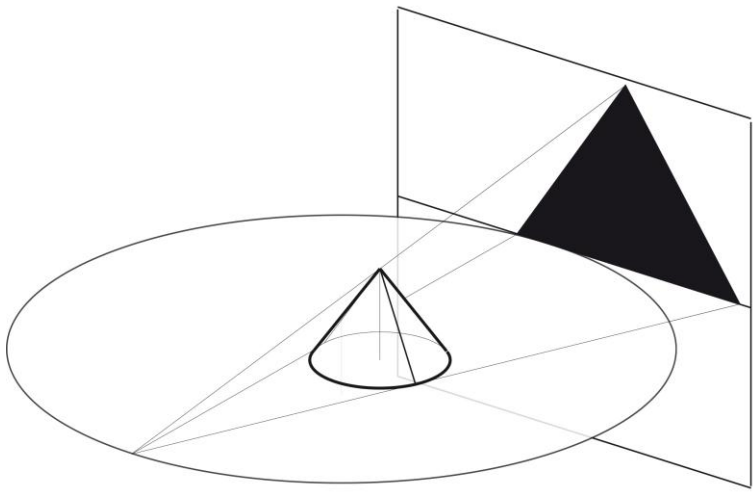

Figure 1. The shadow of the cone

The tangent plane touches the conical surface along the generatrix of the conical surface. Therefore the edges of the shadow of the cone are the projections of the corresponding generatrixes of the conical surface. Since all generatrixes are intersected in the apex of the cone, the projection of the apex can be identified in the image of the cone as the point of the intersection of the edges of the cone shadow. Hence, the first task is to detect the edges of the cone shadow and find the point of their intersection.

There are different approaches that can be used to detect the edges of the cone shadow. One of the most popular among them is the Canny edge detector. Within this approach one seeks for the so called edge pixels of the smoothed image, which are defined as the local maxima of the gradient modulo along the flow curves of the gradient vector field of the smoothed image. Unfortunately the smoothing operation affects the shape of the original shadow, so that the point of the intersection of the edges in the smoothed image may not coincide with the projection of the apex anymore. However, due to the uniform smoothing, the edges of the smoothed shadow remain parallel to the edges of the original (not smoothed) shadow. One can take advantage of this for further correction of the edge position. This is done as follows. Let the desired edge be the segment of the line described by equation

$$t = u\cos\phi + v\sin\phi\,, \tag{1}$$

where only angle ϕ is assumed to be known, and t is not known. The value of parameter t can be obtained from the profile of the grey value image of the shadow, which is defined as the function g represented by samples

$$g(t_k) = I_{i,j} \tag{2}$$

with

$$t_k = u_{i,j}\cos\phi + v_{i,j}\sin\phi\,, \tag{3}$$

where $u_{i,j}, v_{i,j}$ are coordinates of the center of pixel *i,j*, and $I_{i,j}$ is the corresponding grey value of the pixel (see Fig.2).

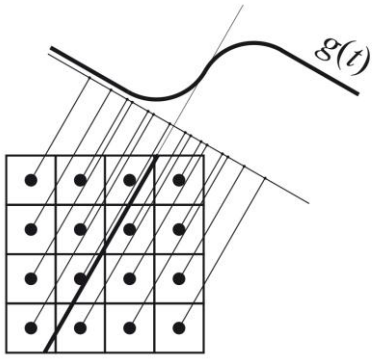

Figure 2. Profile $g(t)$ of the image perpendicular to the edge (bold straight line)

Usually the obtained profile is highly oversampled. Therefore it can be resampled to the regular grid and appropriately smoothed without the risk to affect frequency characteristics of the useful signal contained in the profile. The *t*-value where the slope of the smoothed profile achieves its maximum is assumed to be the desired value of *t* in Eq.1.

2.2 Determination of misalignment of the detector

Ideally the detector plane is parallel to the rotation axis, and the rows of the detector are parallel to the central plane. Misalignments in the imaging system can lead to the deviation of the detector from its ideal position. This deviation can be described by two angles. The first one is the angle between the detector plane and the rotation axis (angle β in Fig. 3), and the second one is the angle between a row of the detector and the line of the intersection of the detector plane and the central plane (line *l* in Fig.3). We denote this angle by θ.

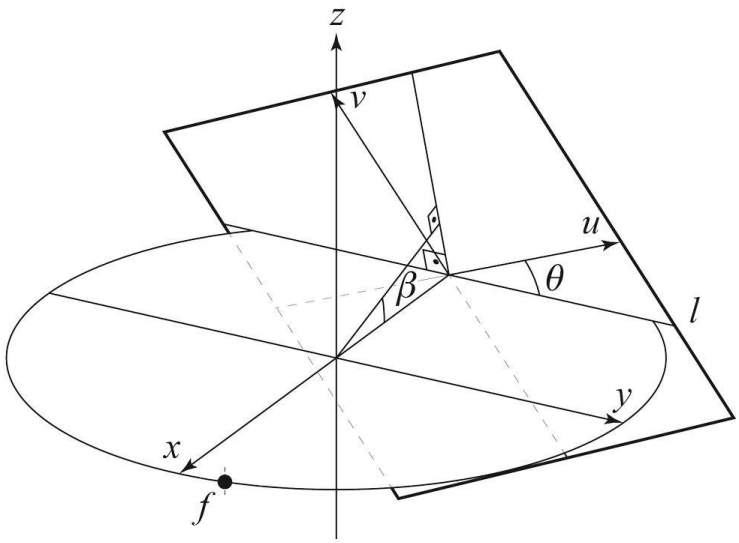

Figure 3. Geometry of the misaligned tomographic system. Here (x,y) is the central plane, z is the rotation axis, f is the focus of the x-ray source, and (u,v) is the detector reference system. Line l is the line of the intersection of the detector and the central plane; β and θ are two typical misalignments of the detector, where β is the tilt of the detector relative to the rotation axis, and θ is the angle between a row of the detector and line l.

The deviation of the angle θ from zero inevitably leads to artefacts in the reconstructed image if the value of θ is not known. Therefore the value of this angle has to be determined. This becomes easy task if the line *l* is identified. The identification of the line *l* is based on the following preposition.

Preposition: Let the central plane be denoted by π. Denote by Π the plane that is parallel to the central plane π, such that $\pi \bigcap \Pi = \varnothing$. Consider in Π parallel lines l_1 and l_2, and denote by d_1 and d_2 their projections onto the detector plane respectively (see Fig.4).
If l_1 and l_2 are not parallel to the detector plane then d_1 and d_2 are not parallel to each other, and $d_1 \bigcap d_2 = q \in l$.
Proof: Let π_1 be the plane that contains line l_1 and focus *f*, and let π_2 be the plane that contains line l_2 and focus *f*. Since $\pi_1 \bigcap \pi_2 \neq \varnothing$ (*f* is the common for them) and $\pi_1 \neq \pi_2$, their intersection is the line that lies in π and is parallel to lines l_1 and l_2. Denote this line by l_3. Apparently, the line l_3 intersects the detector plane in point $q \in l$. Therefore $d_1 \bigcap d_2 = q$.

This preposition is illustrated in Fig.4, where the detector plane is supplied with the reference system *uv*; the line *l* coincides with axis *u*; the central plane is depicted as the big circle.

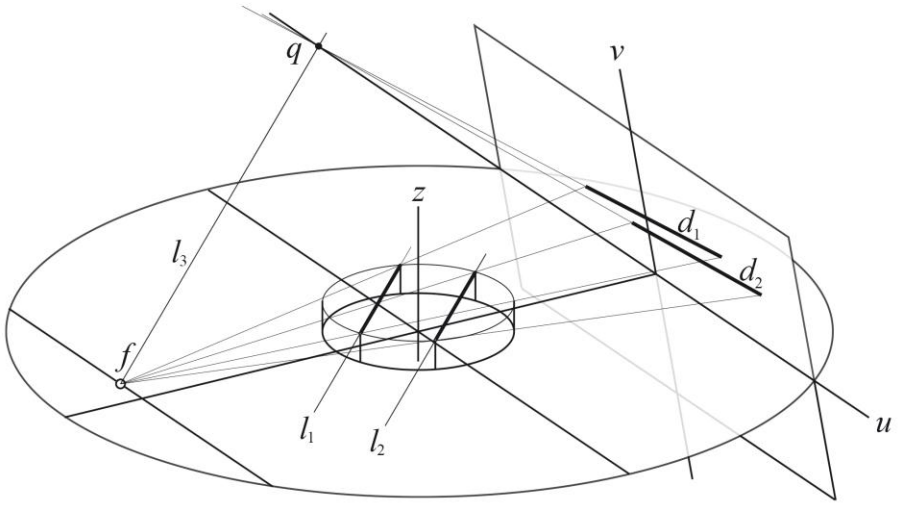

Figure 4. Parallel lines l_1 and l_2 lie in the plane Π such that $\Pi \bigcap \pi = \varnothing$, where π is the central plane. The lines are projected into lines d_1 and d_2 in the detector plane coordinated with *u,v*. Lines d_1 and d_2 intersect each other in point $p \in l$, where l is the line of the intersection of the central plane and the detector plane.

Thus, in order to recover the line *l*, one has to find at least two of its points. As it follows from the above preposition a family of parallel lines in Π relates to the point of the line *l*, and this point is unique. Therefore, in order to find two different points of the line *l*, one has to consider two different families of parallel lines in Π. It is clear that each family has to consist of at least two parallel lines. For example, four sides the square with the center in the origin *O* provide us with the set of necessary lines (see Fig.5). This can easily be realized in the practice. Indeed, the corners of the square

may be four positions of the calibration point rotated successively around the rotation axis at angle $k\pi/2$ for $k = 0,1,2,3$ (see Fig.5).

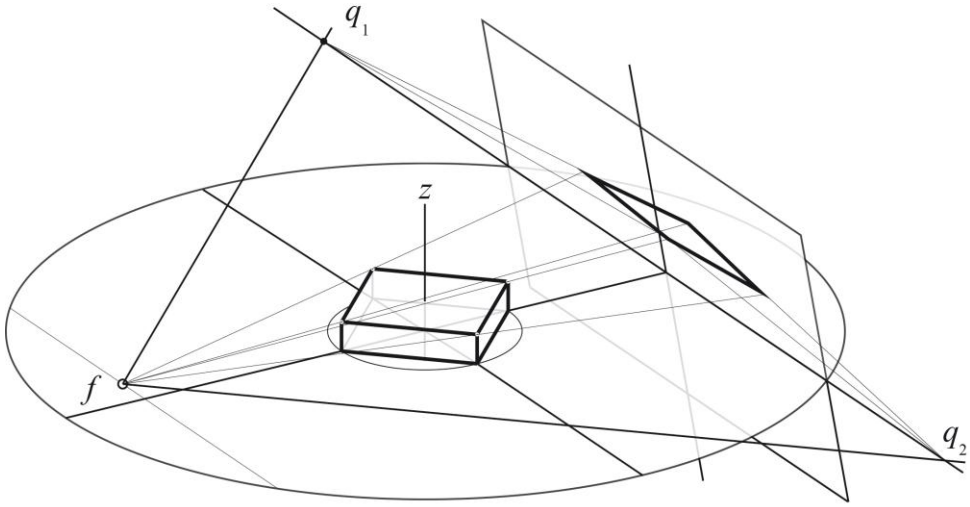

Figure 5. Projection of the square onto the detector plane. The square is depicted as the upper surface of the parallelepiped whose base coincides with the central plane. The projection is the quadrilateral whose opposite sides are not parallel to each other. They are intersected in the points q1 and q2 which generate the line *l*.

3. RESULTS

3.1 Estimation of the projection of the apex

An image of a conic object has been simulated with the Monte Carlo method assuming a x-ray focal spot size 20 microns, detector pixel size of 100 microns. The obtained image is shown in Fig.6 (left). Edge pixels of the cone image have been detected within the manually chosen rectangular regions which are marked with red color in Fig.6 (right).

Figure 6. Left: Monte Carlo simulation of the shadow of the high density conic body; right: edge pixels within marked regions are shown as bold white lines.

Thereafter straight lines have been fitted to the detected edge pixels, yielding line equations in the reference system of the detector. The coordinates of the intersection point of these lines, which is the projection of the apex, are determined simply by solving linear system given by the line equations.

In order to find the line of intersection we use the property according to which projections of space lines, which are both mutually parallel and parallel to the (*x*,*y*)-plane, intersect in a point lying on the line of intersection. Therefore, in order to find the line of intersection it is enough to acquire four projections of the cone, each obtained after subsequent rotations of the cone by 90° around the *z*-axis. Then the projections of the cone apex constitute a quadrilateral whose opposite sides, if extended, are intersected in points lying on the line of intersection. In such a manner one can find as many points of the line of intersection as necessary for a desired precision. In this paper the analysis is restricted to find two points only.
Using the method described above coordinates of the cone apex' projection have been measured several times, each time edge pixels were detected within newly chosen regions. The calculated coordinates have been compared with the theoretically exact coordinates of the cone apex' projection. The results given in pixel-units are shown in table 1

Table 1. Nine measurements of the (*u*,*v*)-coordinates of the intersection point of the lines which best fit edge pixels within manually chosen regions; values *du* and *dv* are errors of measurements, i.e. *du*=*u*-*u*0, *dv*=*v*-*v*0, where *u*0 and *v*0 are true coordinates of the projection of the cone apex.

	Measurement no.								
	1	2	3	4	5	6	7	8	9
u	212.7895	212.8125	212.8158	212.7948	212.7886	212.8034	212.8002	212.8080	212.7942
du	-0.01049	0.01249	0.01579	-0.00520	-0.01139	0.00340	0.00019	0.00799	-0.00579
v	376.6898	376.7457	376.6677	376.7521	376.7019	376.6911	376.6895	376.6937	376.7164
dv	-0.01022	0.04568	-0.03231	0.05209	0.00189	-0.00891	-0.01049	-0.006317	0.01638

3.2 Estimation of the detector tilt

We have applied the method described in a) for estimating angle θ between a row of the detector pixels and the line of intersection (line *l* in Fig.3) of the detector and the (*x*,*y*)-plane, i.e. the plane that contains the focus of the x-ray source and that is perpendicular to the system rotation axis, also known as *z*-axis (see Fig.2).

For this paper four projections of the conic body, each corresponding to the position obtained after subsequent rotation of the body by 90° around the *z*-axis, have been simulated for the arrangement with the detector rotated by angle $\theta = 2°$ around its normal. Projections of the cone apex have been obtained using the method described in item a) of section Methods. Using the method described in b), two points $q_1 = (u_1, v_1)$ and $q_2 = (u_2, v_2)$ which define the line *l* of intersection have been calculated. The desired angle θ has been calculated using formula

$$\tan\theta = \frac{v_2 - v_1}{u_2 - u_1}$$

from which the following value has been obtained for our example

$$\theta = 2.007°$$

4. CONCLUSION

Many techniques proposed for measuring misalignments in cone-beam CT imaging system are based on observing projections of small high-density balls. As described in section Description of Purpose, the identification of the projection of a ball's center is an entirely not trivial task, and can create significant measurement errors. In the approach proposed in this paper, the point whose projection must be identified is not the center of a ball but the apex of a cone

made of some high-density material. Since straight line segments forming the conical surface converge to its apex, the projection of the apex can be identified as the point of intersection of straight lines which best fit edge pixels of the shadow cast by the cone on the detector. This approach has two advantages: A conic body as such can easily be manufactured with high precision and the processing routine necessary for the identification of the desired point in the image of the cone is much simpler and more robust than the one used to identify the projection of the center of a ball. In the paper we have exemplarily applied the method to estimate a misalignment in a cone-beam CT system caused by a small rotation of the detector around its normal. It is known that this misalignment can cause severe artefacts in the reconstruction of an object obtained from a set of cone-beam projections. It has been shown that even with a minimal number of measurements this misalignment can be determined with a high degree of accuracy. This can be explained by the very small magnitude of measurement errors.

REFERENCES

[1] Gullberg G.T., Tsui B.M., Crowford C.R., Ballard J.G., Hagius J.T., "Estimation of geometrical parameters and collimation evaluation for cone beam tomography," Med. Phys. 17(2), 264-272, (1990)

[2] Noo F., Clackdoyle R., Mennessier C., White T.A., Roney T.J., "Analytic method based on identification of ellipse parameters for scanner calibration in cone-beam tomography," Phys Med Biol. 45(11),3489-508 (2000).

[3] Zhao J., Hu X., Zou J., "Geometric Parameters Estimation and Calibration in Cone-Beam Mirco CT," Sensors (Basel). 15(9), 22811-25 (2015)